Title

Understanding trends in C–H bond activation in heterogeneous catalysis

Journal

Nature Materials, 16(2)

ISSN

1476-1122

Authors

Latimer, Allegra A
Kulkarni, Ambarish R
Aljama, Hassan
et al.

Publication Date

2017-02-01

DOI

10.1038/nmat4760

Peer reviewed

Understanding Trends in C-H Bond Activation in Heterogeneous Catalysis

Allegra A. Latimer,[1,‡] Ambarish R. Kulkarni,[1,‡] Hassan Aljama,[1] Joseph H. Montoya,[3] Jong Suk Yoo,[1] Charlie Tsai,[1] Frank Abild-Pedersen,[1,2] Felix Studt,[1,2] Jens K. Nørskov[1,2,*]

[1] SUNCAT Center for Interface Science and Catalysis, Department of Chemical Engineering, Stanford University, 450 Serra Mall Stanford, California 94305, USA

[2] SUNCAT Center for Interface Science and Catalysis, SLAC National Accelerator Laboratory, 2575 Sand Hill Road, Menlo Park, California 94025, United States

[3] Environmental Energy Technologies Division, Lawrence Berkeley National Laboratory, 1 Cyclotron Road, Berkeley, California 94720, USA

* corresponding author: norskov@stanford.edu

‡ equal contribution

While the search for catalysts capable of directly converting methane to higher value commodity chemicals and liquid fuels has been active for over a century, a viable industrial process for selective methane activation has yet to be developed.[1] Electronic structure calculations are playing an increasingly relevant role in this search, but large scale materials screening efforts are hindered by computationally expensive transition state barrier calculations. The purpose of the present letter is two-fold. First, we show that, for the wide range of catalysts that proceed *via* a radical intermediate, a unifying framework for predicting C-H activation barriers using a single universal descriptor can be established. Second, we combine this scaling approach with a thermodynamic analysis of active site formation to provide a map of methane activation rates. Our model successfully rationalizes the available empirical data and lays the foundation for future catalyst design strategies that transcend different catalyst classes.

Methane is relatively inert, and many different classes of catalysts have been investigated for its activation. In all catalyst materials, one of two distinct transition state (TS) geometries is observed[2] (Figure S1). For some catalysts, such as non-noble metals and certain oxides, unsaturated surface atoms are available to stabilize the methyl group in the TS[3–6]. However, if the CH_3-surface interaction is energetically unfavorable[7] or geometrically inaccessible[8], a radical-like TS is observed[2,9–13]. Many of the most promising catalysts for alkane activation fall into this second category: cation-exchanged zeolites[11,14–17], Metal Organic Frameworks (MOFs)[18,19] and decorated graphene nanosheets (GN)[20] for the partial oxidation of alkanes, and certain oxides[2,21] and zeolites[22] for oxidative coupling of methane (OCM).

Hydrogen affinity (E_H) has previously been shown to be a suitable descriptor of reactivity for radical hydrocarbon activation[23–25]. However, these analyses have traditionally been limited to trends within groups of certain transition metal oxides. By examining twenty distinct classes of catalysts, including those as diverse as zeolites, oxides, metals and MOFs, we broaden the scope of these studies and demonstrate that E_H can be used universally to describe all catalysts that follow the radical methane activation mechanism (Figure 1). Here, E_H is defined as:

$$E_H = E(M_m O_x H_{y+1}) - E(M_m O_x H_y) \qquad (1)$$

where, $E(M_m O_x H_{y+1})$ and $E(M_m O_x H_y)$ are the formation energies of the reduced and bare active site, respectively, referenced to gas-phase H_2O and O_2 (Eq. S1). Figure 1 includes a vast range of interesting catalyst materials, and prototypical examples of transition state geometries for several of these materials are shown in Figure 2. For each case, we observe that methane activation proceeds through a radical-like TS. This TS is characterized by a C-H (O-H) bond length of ~ 2.5 (1.2) Å, and its radical nature is

confirmed by examining the carbon-PDOS and spin density difference (Figure S2-S4). We note that other related descriptors have been previously used for similar purposes, including oxide surface reducibility[2], acidity/basicity[26] and reaction energy[4,27]. However, these trend studies have generally been limited to describing one subset of catalyst materials in their analysis.

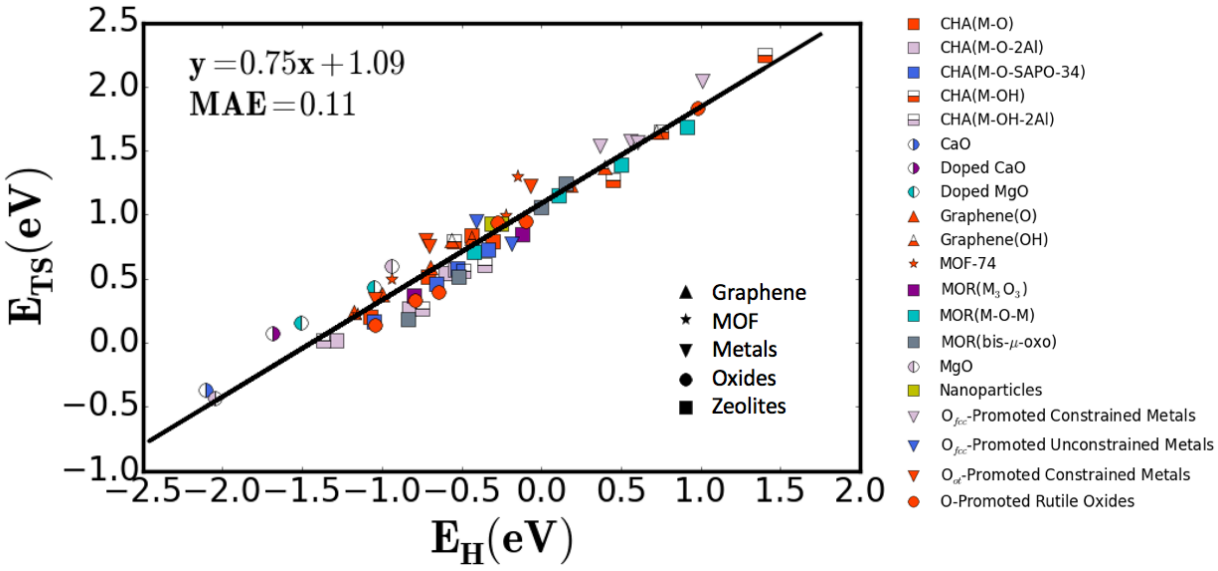

Figure 1. Universal scaling relationship for methane C-H bond activation that proceeds *via* a radical TS. Filled symbols correspond to M-O active sites, while half-filled symbols correspond to M-OH active sites. Legend shows classes of materials explored, and within each class several metals or cations were considered. Maximum absolute error is 0.3 eV, and mean absolute error (MAE) is 0.11. For a description of each material class, see Table S1. For a complete list of energies see Table S2.

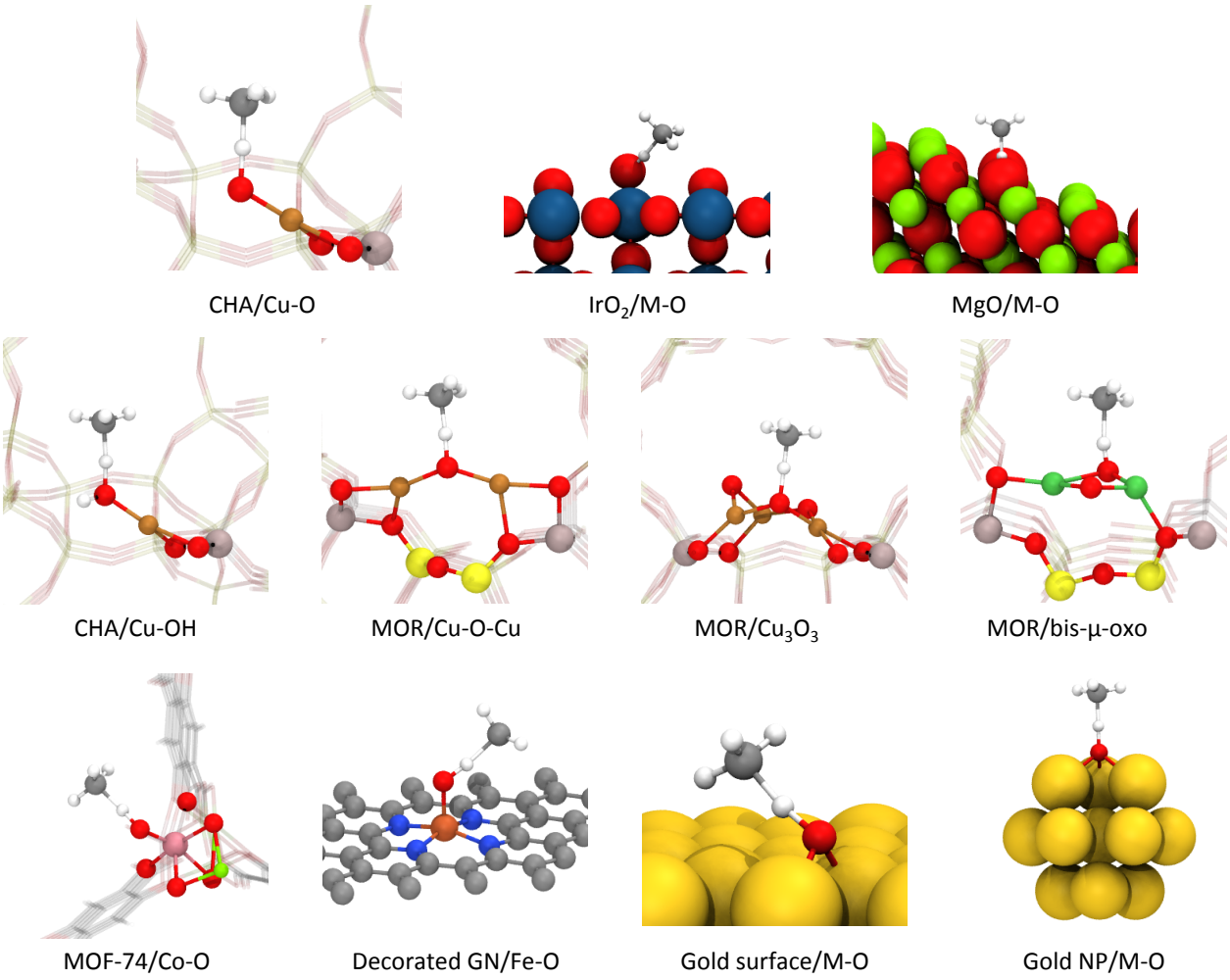

Figure 2. Transition state geometries for various active site motifs. DFT calculated methane activation transition states for several prototypical catalysts all showing a methyl-radical geometry.

Similar to the above analysis, we determined the TS and universal scaling lines for C-H bond activation in ethane and methanol for different active sites and materials using the same descriptor, E_H. The universal scaling lines for these reactants lie below and parallel to the methane activation line (Figure 3(a)). Inspired by the recent work on metal surfaces, we expect the shift in TS scaling for different reactants to be related to the reactant's C-H bond strength, $E_{C\text{-}H}$[28]. Figure 3(b) illustrates this relationship for Fe/(Mg) MOF-74[18,19] for C_1-C_3 alkanes and methanol. Using this relationship, we can describe C-H bond activation across reactants and catalysts by a more general equation (Eq. 2) that depends only on the hydrogen affinity of the catalyst and the C-H bond energy of the reactant.

$$E_{TS} = 0.75E_H - 1.26E_{C-H} - 4.93 \qquad (2)$$

Figure 3(c) demonstrates the excellent agreement between the model's predictions and calculated DFT C-H bond activation energies across a wide variety of reactants and catalyst.

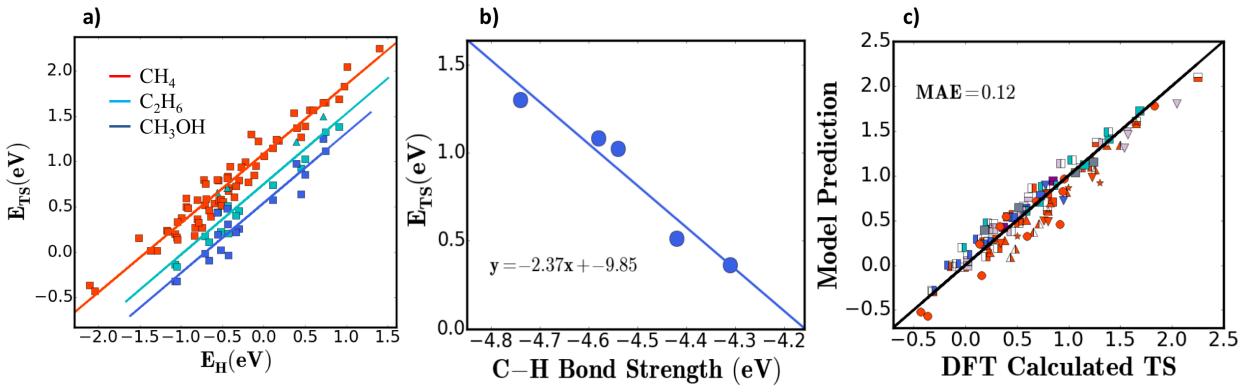

Figure 3. C-H bond activation for different adsorbates. (a) Universal scaling for C-H activation of methane ($E_{TS} = 0.75E_H + 1.09$, $MAE = 0.11$), ethane ($E_{TS} = 0.75E_H + 0.7$, $MAE = 0.13$) and methanol ($E_{TS} = 0.75E_H + 0.54$, $MAE = 0.12$). (b) The activation energies of C_1-C_3 alkanes and methanol on Fe(Mg)/MOF-74 plotted as a function of C-H bond energies. (c) Comparison of DFT-calculated transition state energies and the model predictions for methane, ethane, and methanol activation for all catalysts materials considered.

It is useful to examine the implications of accurately predicting C-H activation energies for many reactants for a large library of chemically and structurally diverse catalyst materials (Figure 2) using a single descriptor. The errors for the scaling relationships shown in Figure 1 and Figure 3(a) (~ 0.1 eV) are comparable to the typical accuracy of DFT adsorption energies[29,30]. More importantly, these small deviations indicate that computationally expensive calculations of TS energies can be avoided, and this model can easily be used to accelerate materials discovery for various C-H bond activation reactions. Our findings also support the well-established idea[1] that selective methane to methanol oxidation in a continuous catalytic process is problematic due to the more facile activation of methanol over methane for a given active site, suggesting that step-wise processes analogous to those used in zeolite chemistry may be required to achieve selectivity.

With the insight that a single descriptor can be used to predict C-H activation energies on many diverse catalyst materials, we are able to generate a simple model of the ability of a catalyst to activate methane. Therefore, we shift our focus to free energies, as these are more relevant for a reaction rate analysis. While we acknowledge that the ability to activate methane is only one of the necessary characteristics of an ideal alkane activation catalyst, we choose not to focus on product selectivity as the

complex nature of selectivity would hinder a general analysis across catalyst classes. The rate of methane activation can be written as:

$$rate = \vartheta_{motif} \frac{k_b T}{h} exp\left(\frac{-\Delta G_a}{RT}\right) \quad (3)$$

Where, ϑ_{motif} is the fraction of available active sites of the catalytic material and the remaining terms express the rate of molecular methane activation. Note that Eq. (3) is a simple measure of activity assuming only one type of active site that may not be directly related to the overall performance of the catalyst. This is an important distinction, as the overall activity of a catalyst will depend on the material properties, synthesis method, and other possible species that can be formed during activation. For instance, during zeolite activation for partial oxidation of methane, different oxygen containing species can be formed to varying degrees depending on the Si/Al ratio, extent of cation exchange, Al distribution, cation positions and zeolite topology. Although a detailed investigation of these factors is beyond the scope of this work, we acknowledge that the ϑ_{motif} represents an upper bound of the equilibrium active site coverage for the specific materials we have considered. ϑ_{motif} is a function of the free energy of active site formation, G_f. The forms of these functions, which will change for different active site geometries and oxidizing agents, are given in Eq. S2-S7. If only M-O actives sites are considered with molecular oxygen as the oxidant, G_f and ϑ_{motif} can be generally defined as follows:

$$G_f(M_mO_x) = G(M_mO_x) - \left(\frac{1}{2}\right) G(O_2) - G(M_mO_{x-1}) \quad (4)$$

$$\vartheta_{motif} = \frac{\sqrt{P_{O2}} e^{-G_f/k_B T}}{1+\sqrt{P_{O2}} e^{-G_f/k_B T}} \quad (5)$$

A plot of ϑ_{motif} as a function of G_f for oxygen activation of MO active sites is given in Figure S5. For simplicity, only materials with M-O active sites activated *via* molecular oxygen for the methane oxidation reaction are explored in the following discussion. A similar analysis of M-OH active site materials and other oxidants is presented in Figures S6-7.

Given that the TS energy scales with the hydrogen affinity (Figure 1), G_f and G_H provide a complete description of the ability of a catalyst to activate methane. G_H is defined analogously to E_H as:

$$G_H = G(M_mO_xH_{y+1}) - G(M_mO_xH_y) \quad (6)$$

where $G(M_mO_xH_{y+1})$ and $G\left(M_mO_xH_y\right)$ are the formation free energies of the reduced and bare active sites referenced to the gas-phase free energies of H_2O and O_2. Using these quantities as independent descriptors, a two-dimensional rate volcano can be constructed showing the rate of methane activation as a function of G_f and G_H (Figure 4(a)). Here, we focus on low temperature (150 °C) methane activation, which is primarily relevant to partial methane oxidation to methanol. Therefore, $\boldsymbol{\Delta}G_a$ in Eq. 3 is calculated at 150 °C. We model the high temperatures used for catalyst activation in zeolite chemistry by calculating ϑ_{motif} in Eq. 3 at 450 °C. However, we note that the results are not significantly different if oxygen equilibration takes place at 150 °C or 600 °C, or if N_2O is used as an oxidant (Figure S7).

Interestingly, all the materials explored seem to fall on one of two distinct G_f vs. G_H scaling lines (red and purple lines, Figure 4(a)). We posit the physical origin of these two lines may be related to the ability of the substrate to delocalize changes in charge following active site formation, as determined by a Bader charge analysis before and after oxygen adsorption to form the active site (Figures S8-S11). Along each G_f vs. G_H scaling line, the dimensionality of the problem is reduced to a single independent descriptor and a one-dimensional rate volcano can be generated (Figure 4(b)). Materials that fall on the lower G_f vs. G_H scaling line (the high activity class, red line) include various active site motifs for zeolites and several oxygen-promoted rutile oxides. The results clearly explain the prevailing interest in Cu-exchanged zeolites, as Cu-exchanged catalysts tend to be closer to the peak of the volcano than other cations for a given active site motif (Figure 4(b)). These include the previously studied Cu-O-Cu/MOR,[11] bis-μ-oxo Cu/MOR,[17] and Cu_3O_3/MOR[16] motifs. This finding is especially relevant given that Cu_3O_3/MOR (purple square, Figure 4(b)) was recently demonstrated to have an order of magnitude greater methanol yield (per Cu atom) than other zeolites[16]. Additionally, certain materials that, to the best of our knowledge, have not yet been tested for partial oxidation of methane, such as oxygen promoted IrO_2, also lie close to the peak of the volcano. It should be stressed that this volcano only elucidates the ability of a catalyst to break the initial C-H bond in methane, and is meant to serve as a guide in the initial stages of catalyst discovery. We do not claim that materials near the peak of the volcano such as IrO_2 will be selective to methanol formation, but instead suggest that IrO_2 is likely to have high methane activation activity at low temperatures. While a new catalyst's selectivity must be explored separately, this simple kinetic and thermodynamic model can provide a useful foundation for easily evaluating the often rate-limiting crucial first step in methane oxidation.

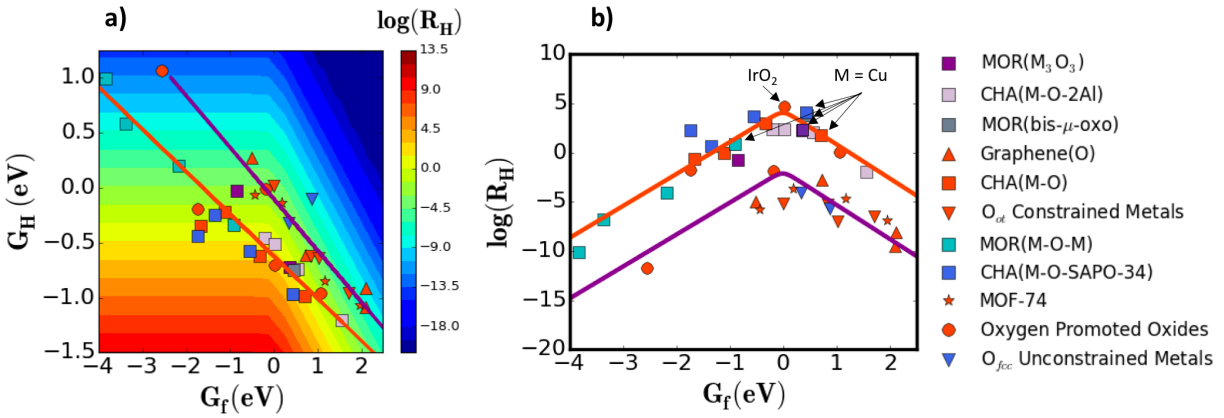

Figure 4. Volcano plots for methane activation. (a) 2-D volcano that includes G_H and G_f as descriptors for all explored materials and **(b)** 1-D volcano plot for the intrinsic rate of methane activation using G_f as a descriptor. An active site formation temperature of 450 °C and a methane activation temperature of 150 °C are used. All rates are theoretical values calculated using Eq. 3.

For computational screening approaches to be viable for materials discovery, suitable scaling relationships that avoid the computationally expensive calculation of TS energies are necessary. Traditionally, most of the reported descriptor approaches have been limited to describing one reaction within a single class of catalyst materials[2,23–26]. In this work, we have shown that hydrocarbon activation provides a unique opportunity for the development of a universal scaling relationship that accurately describes a vast library of catalyst materials and reactions, which has not been previously demonstrated. We postulate that this is possible because the radical-like transition state interacts with only one site on the catalyst surface, and, therefore, does not depend significantly on catalyst geometry.

Our analysis provides the guidelines necessary to predict and compare the performance of new catalysts with the existing materials used for C-H bond activation reactions. One approach to improving activity is to tune the formation energy of the active site motif (ΔG_f) by changing the physical characteristics of the catalyst. We illustrate this approach by evaluating different zeolite topologies (AEI, AFX, MAZ, MOR, FAU), including 4d and 5d transition metal cations for M-O/CHA motif, inducing strain in IrO_2 and evaluating perovskites for C-H activation. Figure 5 shows that all of these materials follow one of the two scaling lines identified earlier, and many fall in the high activity region of the volcano plot (details in Table S1). While the provided analysis does not guarantee any of these materials to be selective to partial oxidation, it does answer the question of whether methane will be activated at a given temperature. Undoubtedly, many catalysts that are able to activate methane at low temperatures will have poor selectivity, but no catalyst that fails to activate methane can go on to be selective. The methods presented herein are meant to quickly determine whether a new material of interest can

successfully activate methane and should be examined further. Only once the question of methane activation is answered can the difficult problem of selectivity be explored.

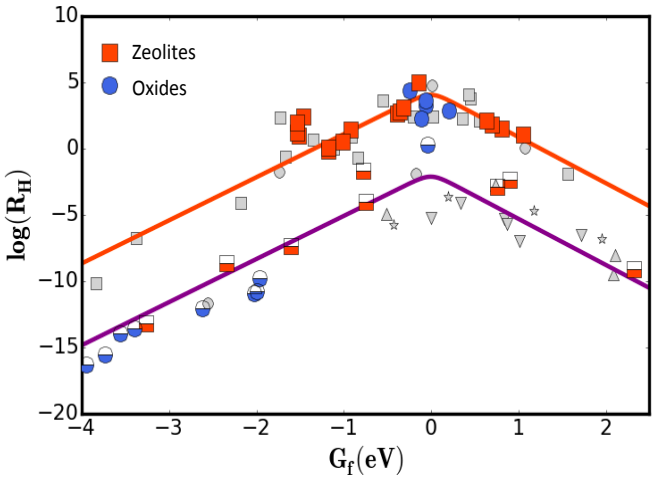

Figure 5. Identifying promising catalysts for methane activation using scaling. Rate volcano for different zeolite topologies (AEI, AFX, MAZ, MOR, FAU) for M-O active site motif (red squares), 4d and 5d transition metal cations for M-O/CHA (half-filled red squares) and oxides (perovskites and strained IrO_2, blue circles). The filled symbols correspond to systems for which a TS was explicitly calculated using DFT and half-filled symbols represent the rates predicted by the universal scaling relationship. Grey points are the original set of materials shown in Figure 4.

Acknowledgements
Support from the U.S. Department of Energy Office of Basic Energy Science to the SUNCAT Center for Interface Science and Catalysis is gratefully acknowledged. The research of AAL was conducted with Government support under and awarded by DoD, Air Force Office of Scientific Research, National Defense Science and Engineering Graduate (NDSEG) Fellowship, 32 CFR 168a. ARK acknowledges the computing resources from Carbon High-Performance Computing Cluster at Argonne National Laboratory under proposal CNM-46405. CT acknowledges support from the National Science Foundation Graduate Research Fellowship Program (GRFP) Grant DGE-114747. JHM acknowledges funding from the NSF GRFP, grant number DGE-114747, and also the Center of Nanostructuring for Efficient Energy Conversion (CNEEC) at Stanford University, an Energy Frontier Research Center funded by the U.S. Department of Energy, Office of Basic Energy Sciences under award number DE-SC0001060. JSY appreciates the financial support from US DOS via International Fulbright Science & Technology Award program. HA receives funding from Aramco Services Company.

References

1. Horn, R. & Schlogl, R. Methane Activation by Heterogeneous Catalysis. *Catalysis Letters* **145,** 23:39 (2014).
2. Kumar, G., Lau, S. L. J., Krcha, M. D. & Janik, M. J. Correlation of Methane Activation and Oxide Catalyst Reducibility and Its Implications for Oxidative Coupling. *ACS Catal.* 1812–1821 (2016).
3. Wang, C. C., Siao, S. S. & Jiang, J. C−H Bond Activation of Methane via σ−d Interaction on the IrO_2(110) Surface: Density Functional Theory Study. *J. Phys. Chem. C* **116,** 6367–6370 (2012).
4. Yoo, J. S., Khan, T. S., Abild-Pedersen, F., Nørskov, J. K. & Studt, F. On the role of the surface oxygen species during A–H (A = C, N, O) bond activation: a density functional theory study. *Chem. Commun.* **51,** 2621–2624 (2015).
5. Weaver, J. F., Hakanoglu, C., Antony, A. & Asthagiri, A. Alkane activation on crystalline metal oxide surfaces. *Chem. Soc. Rev.* **43,** 7536–7547 (2014).
6. Antony, A., Asthagiri, A. & Weaver, J. F. Pathways and kinetics of methane and ethane C-H bond cleavage on PdO(101). *J. Chem. Phys.* **139,** (2013).
7. Abild-Pedersen, F. *et al.* Scaling properties of adsorption energies for hydrogen-containing molecules on transition-metal surfaces. *Phys. Rev. Lett.* **99,** 4–7 (2007).
8. Li, B. & Metiu, H. Dissociation of Methane on La_2O_3 Surfaces Doped with Cu, Mg, or Zn. *J. Phys. Chem. C* **115,** 18239–18246 (2011).
9. Krcha, M. D., Mayernick, A. D. & Janik, M. J. Periodic trends of oxygen vacancy formation and C–H bond activation over transition metal-doped CeO_2 (111) surfaces. *J. Catal.* **293,** 103–115 (2012).
10. Schwarz, H. Chemistry with methane: Concepts rather than recipes. *Angew. Chemie - Int. Ed.* **50,** 10096–10115 (2011).
11. Woertink, J. S. *et al.* A $[Cu_2O]^{2+}$ core in Cu-ZSM-5, the active site in the oxidation of methane to methanol. *Proc. Natl. Acad. Sci. U. S. A.* **106,** 18908–18913 (2009).
12. Da Silva, J. C. S., Pennifold, R. C. R., Harvey, J. N. & Rocha, W. R. A radical rebound mechanism for the methane oxidation reaction promoted by the dicopper center of a pMMO enzyme: a computational perspective. *Dalt. Trans.* Advance Online Publication, doi:10.1039/C5DT02638E (2016).
13. Chin, Y. H., Buda, C., Neurock, M. & Iglesia, E. Consequences of metal-oxide interconversion for C-H bond activation during CH4 reactions on Pd catalysts. *J. Am. Chem. Soc.* **135,** 15425–15442 (2013).
14. Wulfers, M. J., Lobo, R. F., Ipek, B. & Teketel, S. Conversion of Methane to Methanol on Copper-Containing Small-Pore Zeolites and Zeotypes. *Chem. Commun.* **51,** 4447–4450 (2015).
15. Hammond, C. *et al.* Direct catalytic conversion of methane to methanol in an aqueous

medium by using copper-promoted Fe-ZSM-5. *Angew. Chemie - Int. Ed.* **51,** 5129–5133 (2012).

16. Grundner, S. *et al.* Single-site trinuclear copper oxygen clusters in mordenite for selective conversion of methane to methanol. *Nat. Commun.* **6,** 7546 (2015).
17. Groothaert, M. H., Smeets, P. J., Sels, B. F., Jacobs, P. A. & Schoonheydt, R. A. Selective Oxidation of Methane by the Bis (μ -oxo) dicopper Core Stabilized on ZSM-5 and Mordenite Zeolites. *J. Am. Chem. Soc.* **127,** 1394–1395 (2005).
18. Verma, P. *et al.* Mechanism of oxidation of ethane to ethanol at Iron(IV)-oxo sites in magnesium-diluted Fe_2(dobdc). *J. Am. Chem. Soc.* **137,** 5770–5781 (2015).
19. Xiao, D. J. *et al.* Oxidation of ethane to ethanol by N_2O in a metal-organic framework with coordinatively unsaturated iron(II) sites. *Nat. Chem.* **6,** 590–5 (2014).
20. Impeng, S. *et al.* Methane activation on Fe- and FeO-embedded graphene and boron nitride sheet: role of atomic defects in catalytic activities. *RSC Adv.* **5,** 97918–97927 (2015).
21. Sun, X., Li, B. & Metiu, H. Methane dissociation on Li-, Na-, K-, and Cu-doped flat and stepped CaO(001). *J. Phys. Chem. C* **117,** 7114–7122 (2013).
22. Lu, Y. *et al.* A high coking-resistance catalyst for methane aromatization. *Chem. Commun. (Camb).* 2048–2049 (2001).
23. Tyo, E. C. *et al.* Oxidative Dehydrogenation of Cyclohexane on Cobalt Oxide (Co_3O_4) Nanoparticles: The Effect of Particle Size on Activity and Selectivity. *Acs Catal.* **2,** 2409–2423 (2012).
24. Atzkern, S., Borisenko, S., Knupfer, M. & Golden, M. Valence-band excitations in V_2O_5. *Phys. Rev. B* **5,** 5849–5852 (2000).
25. Fu, G., Chen, Z. N., Xu, X. & Wan, H. L. Understanding the reactivity of the tetrahedrally coordinated high-valence d^0 transition metal oxides toward the C-H bond activation of alkanes: A cluster model study. *J. Phys. Chem. A* **112,** 717–721 (2008).
26. Chen, K., Xie, S., Bell, A. T. & Iglesia, E. Alkali Effects on Molybdenum Oxide Catalysts for the Oxidative Dehydrogenation of Propane. *J. Catal.* **195,** 244–252 (2000).
27. Tsai, C., Latimer, A. A., Yoo, J. S., Studt, F. & Abild-Pedersen, F. Predicting Promoter-Induced Bond Activation on Solid Catalysts Using Elementary Bond Orders. *J. Phys. Chem. Lett.* **6,** 3670–3674 (2015).
28. Karp, E. M., Silbaugh, T. L. & Campbell, C. T. Bond energies of molecular fragments to metal surfaces track their bond energies to H atoms. *J. Am. Chem. Soc.* **136,** 4137–4140 (2014).
29. Medford, A. J. *et al.* Assessing the reliability of calculated catalytic ammonia synthesis rates. *Science (80-.).* **345,** 197 (2014).
30. Wellendorff, J. *et al.* Density functionals for surface science: Exchange-correlation model development with Bayesian error estimation. *Phys. Rev. B* **85,** 235149 (2012).

Methods

Metals and Oxides:

The plane wave QuantumEspresso code and Bayesian Error Estimation Functional with Van der Waals corrections (BEEF-vdw) functional was used for the Density Functional Theory (DFT) calculations. All adsorption and transition state energy calculations for metal and oxide surfaces were spin polarized. For adsorption of –O and –OH species, spin polarization did not affect the adsorption energies and non-spin polarized calculations were used. Forces on all atoms were minimized to 0.05 eV $Å^{-1}$. For oxides, perovskites and metals, (6,6,1) k-point sampling was employed. A 2x1 expansion of the 110 surface unit cell is used for oxides and perovskites, while a 3x3 expansion of the 111 surface unit cell was used for metals. Metals, oxides and perovskites slabs were composed of four stoichiometric layers separated by 15 Å vaccum, and the bottom 2 layers were kept fixed to simulate the bulk. For each active site motif and material category, we performed Climbing-Image Nudged Elastic Band (CI-NEB) determine the location of the transition state (TS).

Zeolites, MOFs, Graphenes and Nanoparticles:

All calculations were performed using the BEEF-vdW functional as implemented in the periodic Vienna Ab Initio Simulation (VASP) code. All possible spin multiplicities are considered to determine the ground state electronic configuration. For zeolites, MOFs and nanoparticles only the gamma point was used, while a (3,3,1) k-point sampling was employed for the decorated graphene sheets. Forces on all atoms were converged to 0.03 eV $Å^{-1}$. The initial zeolite structures were obtained from the IZA database (http://www.iza-structure.org/databases/) and the lattice constants were optimized at an energy cutoff of 700 eV. All further geometry optimizations and transition state calculations were performed using fixed unit cell size at a plane wave cutoff of 400 eV. The MOF-74 structures were obtained from Verma et al.[1] and were similarly optimized. For each active site motif and material category shown in Figure 1, Climbing-Image Nudged Elastic Band (CI-NEB) and Dimer method are used to determine the location of the transition states.

Entropic contributions are found to be similar for all materials, so for the purposes of scaling the zero-point energy entropy contributions (at the harmonic approximation) on IrO_2 are used to calculate free energies at various temperatures.